Journal of Thermal Analysis and Calorimetry (2020) 140:1095–1106
https://doi.org/10.1007/s10973-019-08580-3

Design improvement in a stepped solar still based on entropy generation minimization

Shahabeddin Ashtiani[1] · Faramarz Hormozi[1]

Received: 26 May 2019 / Accepted: 11 July 2019 / Published online: 23 July 2019

Abstract

In this numerical study, an entropy generation analysis is performed to optimize the geometry of a stepped solar still through minimization of irreversibilities. The moist air model is used for the simulation of the double diffusive free convection heat transfer inside the stepped solar still. The governing equations are solved by employing a finite volume technique. The influences of some geometrical and operating parameters, including the number and height of the steps and the temperatures of glass ceiling and water surface, on the flow structure, concentration and temperature fields, and different types of irreversibilities inside the solar still are studied. The computational results show that the active sites for generating the irreversibilities are regions near the evaporation and condensation surfaces inside the solar still. The fluid friction and concentration terms have negligible contributions to the irreversibility generation, and the thermal irreversibility is the dominant term in the solar still. All types of irreversibility are intensified by increasing the number or height of the steps. From the view point of irreversibility minimization, the usage of a stepped solar still with lower operating temperatures is recommended. In a solar still with four steps, the viscous, thermal, and concentration irreversibilities increase about 41.55%, 316.43%, and 316.6%, respectively, as the step height increases in the range of 2–5 cm. The viscous, concentration, and thermal irreversibilities increase about 8.2%, 53.5%, and 1.57%, respectively, by increasing the temperatures of the glass ceiling and water surface from T_g = 44 °C and T_w = 49 °C to T_g = 54 °C and T_w = 59 °C.

Keywords Irreversibility · Minimization · Stepped solar still · Moist air model · Double diffusive · Operating temperature

Abbreviations

A	Surface (m^2)
Be	Bejan number (–)
Br	Buoyancy ratio (–)
C	Concentration (kg m^{-3})
D_{AB}	Mass diffusivity (m^2 s^{-1})
C_p	Specific heat capacity (J kg^{-1} K^{-1})
g	Acceleration of gravity (m s^{-2})
h	Height of step (m)
H	Height of still (m)
k	Thermal conductivity (W m^{-1} K^{-1})
l	Length of step (m)
L	Length of still (m)
Le	Lewis number (–)
n	Perpendicular direction (–)
Nu	Nusselt number (–)
P	Pressure (Pa)
Pr	Prandtl number (–)
R	Gas constant (J kg^{-1} K^{-1})
Ra	Rayleigh number (–)
S_g	Irreversibility (W m^{-3} K^{-1})
T	Temperature (K)
U	Velocity (m s^{-1})
x, y	Rectangular coordinates (m)

Greek symbols

α	Thermal diffusivity (m^2/s)
β	Volumetric expansion coefficient (K^{-1})
μ	Dynamic viscosity (kg m^{-1} K^{-1})
ν	Kinematic viscosity (m^2 s^{-1})
ρ	Density (kg m^{-3})
Φ	Moisture ratio (–)

✉ Faramarz Hormozi
fhormozi@semnan.ac.ir

Shahabeddin Ashtiani
Sh_ashtiani@semnan.ac.ir

[1] Department of Chemical, Petroleum, and Gas Engineering, Semnan University, Semnan, Iran

Subscripts/superscripts

ave	Average
c	Concentration
g	Glass ceiling
l	Left
r	Right
th	Thermal
v	Viscous
w	Water
*	Dimensional parameter

Introduction

The shortage of freshwater for livelihood has become a serious problem in most regions of the world and needs prompt attention. Freshwater is necessary for human being and also can be used in agriculture and industrial sectors [1]. About 75% of earth is covered by water. A significant portion of the water available in earth, about 97%, is salty water saved in oceans and lakes [2]. This shows the importance of water desalination techniques to use this large amount of water. Reverse osmosis and electrodialysis are two methods for distillation of saline water. Usually, the costs of fabrication and maintenance for these methods are high and also electrical energy should be consumed to operate them. In addition, these methods have high capacities and as a result, they are not proper for the usage in areas with disperse population [3]. Solar desalination techniques are good alternatives that have an eco-friendly operation. Solar stills are recognized as the simple solar desalination equipment [4]. In most cases, the productivities of solar stills are low and accordingly, many techniques are used to overcome this defect. Selvaraj and Natarajan [2] performed a review on the parameters affecting the productivity and efficiency of different solar stills. It was reported that the efficiency of solar still improves as the water depth in the basin of the still decreases. Moreover, the temperature difference between the water surface and glass ceiling directly affects the efficiency as the condensation and evaporation rates can be improved by increasing this temperature difference. In a review paper, Bait and Si–Ameur [5] investigated the potentials of nanofluids for improving the heat and mass transfer in different solar stills. The results of this study showed that the nanofluids have great solar radiation absorption and thermal futures, which can increase the evaporation rate in the solar stills. Omara et al. [6] focused on the cooling methods of glass ceiling in solar stills. They concluded that the temperature of the glass ceiling can decrease in the range of 6–20 °C, and the productivity of the solar still can enhance about 20% by using the cooling techniques. Note that the condensation rate can be enhanced by employing the cooling techniques. Shukla et al. [7] investigated the potentials of phase change materials for improving the efficiency of solar stills. A momentous observation in this study is that the efficiency of the solar still can substantially improve by integrating solar stills with phase change materials and such devices can work effectively for larger time. In an experimental study, Rashidi et al. [8] enhanced the productivity of a single-slope solar still by placing the sponge layer in the basin of the still. They improved the daily productivity of this solar still up to 17.35% by using the sponge layer. Note that the sponge layer, as the porous material, provides more effective surface for evaporation and solar radiation absorption and accordingly, it can increase the productivity of the still. Manokar and Winston [9] used acrylic sheet as the basin of a solar still. They observed that the heat loss from the basin decreases by using this material and this causes increment in the evaporation rate of the water.

In recent years, the stepped solar stills are widely used because of providing higher productivity as compared with the conventional solar stills. This may be due to two reasons. First, the distance between the evaporation and condensation surfaces in a stepped solar still is small and accordingly, the heat and mass can be transferred faster between two surfaces [10]. Second, the stepwise basin in a stepped solar still creates more effective surface area for heat and mass transfer as compared with the flat one [11]. Some researchers have focused on this type of solar still. Omara et al. [12] improved the efficiency of the stepped solar still by employing internal reflectors. They installed some mirrors on the vertical sides of the steps. Their results showed that the stepped solar still equipped with the mirrors provides about 75% higher productivity as compared with a flap basin solar still. Moreover, the conventional stepped solar still without using the mirrors generates up to 57% higher distilled water in comparison with a flap basin solar still. Abdullah et al. [13] used a solar air heating system and a glass ceiling cooling technique to improve the evaporation and condensation rates inside the stepped solar still. They increased the productivity of solar still around 112% by using these methods. In a numerical study, the effects of nanofluids on the productivity of a stepped solar still have been investigated by Rashidi et al. [14]. They found that the hourly productivity of the solar still enhances about 22% as the solid volume fraction of nanoparticles increases in the range of 0–5%. Saadi et al. [15] used a multi-tray evaporating system inside a stepped solar still to provide more evaporation area. Their results showed that this stepped solar still generates about 104.73% higher daily productivity in comparison with the flap basin solar still. Naroei et al. [16] integrated the photovoltaic thermal system with a stepped solar still. The results of this study revealed that integrating the photovoltaic thermal system

with a stepped solar still improves the energy efficiency and pure water production rate and for other purposes could generate extra electrical power.

The effectiveness of each energy system should not only be based on enhanced first law efficiency. Some irreversibilities occur during the operation of system, which can destruct the useful work and quality of energy in the system. These irreversibilities cannot be identified by the first law of thermodynamics [17]. In engineering, the method for detecting and decreasing thermodynamic irreversibilities is generally named by entropy generation analysis that is based on second law of thermodynamics. This analysis is necessary to have a correct evaluation from each energy system [18]. The researchers have used this analysis for various thermal energy systems [19–21]. Ebrahimi-Moghadam and Jabari Moghadam [22] calculated the entropy generation of a nanofluid flow inside the heat exchanger with wavy walls. They found that the alumina nanoparticles with 4% volume fraction results in 5% increase in the irreversibility. Moreover, it was concluded that the share of the viscous irreversibility increases with increasing the Reynolds number. Ghanbarpour and Khodabandeh [23] performed the entropy generation analysis for a cylindrical heat pipe with nanofluid. Their results indicated that the irreversibility in the heat pipe reduces by using the nanofluid as the working fluid. Sivaraj and Sheremet [24] investigated the entropy generation of ferrofluid free convection heat transfer inside an enclosure. It was found that exerting the magnetic field can decrease the generation of irreversibility inside the enclosure. Bouchoucha et al. [25] investigated the entropy generation of free convection in an enclosure with thick bottom surface. They selected the alumina water as the working fluid. They concluded that the Bejan number boosts as the concentration of nanoparticles increases. Bahiraei et al. [26] performed an entropy generation analysis for the nanofluid flow through pipes enhanced with the double twisted tape inserts. They recommended employing the twisted tape with smaller twisted ratios due to the smaller value of overall irreversibility. Bahiraei and Mazaheri [27] performed an entropy generation analysis for the nanofluid flow inside the minichannel equipped with the chaotic twisted perturbations. Their results showed that the thermal irreversibility and Bejan number reduce as the solid volume fraction of nanoparticles and Dean number increase.

The entropy generation analysis is also widely used for different solar thermal energy systems. Rahman et al. [28] simulated the double diffusive free convection in the solar receiver. They concluded that the heat and mass transfer boosts as the buoyancy ratio and Rayleigh number increase. Javaniyan Jouybari et al. [29] inserted the porous material inside the flat plate solar receiver. They investigated the influences of the porous material on the generation of the irreversibility in the collector. They deduced that using the porous material increases the pressure drop inside the collector, but it has negligible influence on the generation of the irreversibility. Rashidi et al. [30] investigated the entropy generation of nanofluid flow through a solar heating system with the roughed absorber plate. It was found that the thermal irreversibility reduces as the rib height increases. Rashidi et al. [31] used the nanofluid inside a single-slope solar still. They calculated the irreversibilities for this problem. It was concluded that the thermal and viscous irreversibilities increase as the concentration of nanoparticles increases. Rashidi and Esfahani [32] calculated the irreversibilities inside a single-slope solar still. They found that different types of irreversibility increase as the aspect ratio of the solar still increases. The aspect ratio was specified as the ratio of length to the height of the solar still.

The above literature review confirms the superior potentials of stepped solar still over conventional solar stills. Moreover, it is concluded that entropy generation analysis is essential for each energy system. The literature review shows that there is no study about the entropy generation analysis for the stepped solar still. Accordingly, the aim of this study is to optimize the geometry and operating condition of a stepped solar still based on an entropy generation analysis. The problem is simulated by using a moist air model, and the finite volume method is used to solve the governing equations. The number and height of steps and the temperatures of glass ceiling and water surface are selected as the input parameters. The influences of these parameters on the flow structure, concentration and temperature fields, and different types of irreversibility inside the solar still are investigated.

Physical model

Figure 1 discloses the geometry of the stepped solar stills. As shown in this figure, two stepped solar stills with four and five steps are considered for the simulation. Solar stills have right side $H_r = 28.5$ cm, left side $H_l = 8$ cm, and length $L = 57$ cm. Moreover, h and l are the height and length of the steps. Generally, in a solar still, the impure water can be evaporated and vapor rises through the air and condenses on the glass ceiling. In this paper, only the space between the impure water surface and glass ceiling is simulated. Accordingly, the bottom wall in Fig. 1 indicates the impure water surface and the top wall is the glass ceiling of the solar still. Both bottom and top walls have constant temperatures as the phase changes occur on these surfaces during the operation of the solar still. The sidewalls of the solar stills are insulated in terms of heat transfer and concentration. In a solar still, there is the

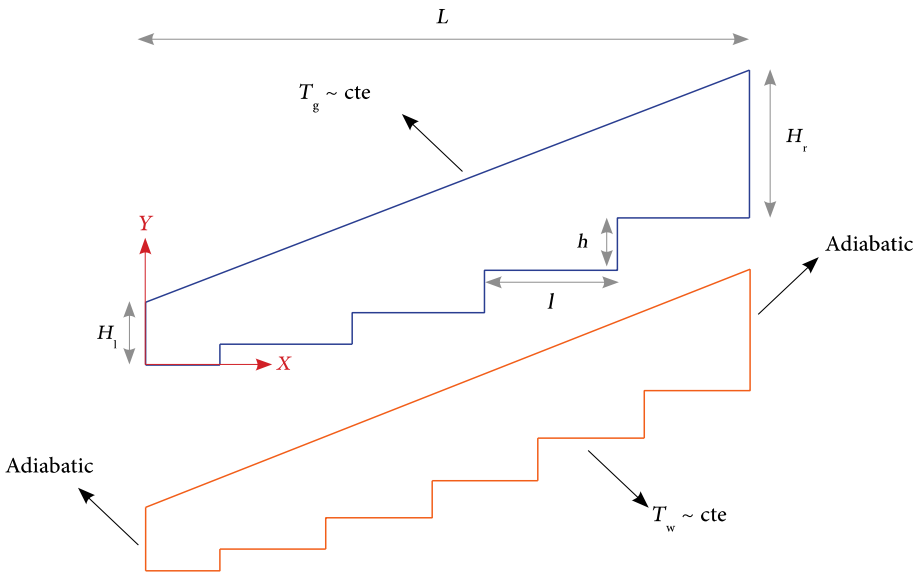

Fig. 1 Solar stills with four and five steps considered for the simulations

double diffusive free convection heat transfer due to both temperature and concentration differences between water surface (evaporation surface) and glass ceiling (condensation surface). Indeed, double diffusive free convection heat transfer is responsible for transferring the heat and mass transfer between condensation and evaporation surfaces. The following assumptions are used for the simulation of this problem:

- Two-dimensional laminar and steady flow is simulated.
- The working fluid is moist air, which can be considered as an ideal gas. Moreover, it is assumed that the moist air is incompressible and has constant thermo-physical properties.
- The viscous dissipation is insignificant.
- The Soret and Dufour effects are not considered.

The thermo-physical properties of the moist air can be calculated by the equations presented in Table 1 [33]. Note that these properties are provided in the average working temperature of the solar still ($\frac{T_g+T_w}{2}$). In this table, T_g and T_w are the temperatures of glass ceiling and water surface, respectively.

Computational model

Governing equations

The governing equations including continuity, momentum, concentration, and energy equations should be solved to calculate the velocities, temperature, and concentration inside the solar still. By using the assumptions provided in the previous section, the governing equations are [34].

Table 1 Thermo-physical properties of the moist air used in the simulation [27]

Property	Equation
Density	$\rho = 353.44/\left(\left(\frac{T_g+T_w}{2}\right) - 273.15\right)$
Expansion factor	$\beta = 1/\left(\left(\frac{T_g+T_w}{2}\right) - 273.15\right)$
Specific heat capacity	$c_p = 999.2 + 0.1434 \times \left(\frac{T_g+T_w}{2}\right) + 1.101 \times 10^{-4} \times \left(\frac{T_g+T_w}{2}\right)^2 - 6.758 \times 10^{-8} \times \left(\frac{T_g+T_w}{2}\right)^3$
Thermal conductivity	$k = 0.0244 + 0.7673 \times 10^{-4} \times \left(\frac{T_g+T_w}{2}\right)$
Viscosity	$\mu = 1.718 \times 10^{-5} + 0.7673 \times 10^{-8} \times \left(\frac{T_g+T_w}{2}\right)$

Dimensional form

Continuity equation:

$$\nabla^* \cdot \mathrm{U}^* = 0 \tag{1}$$

Note that superscript * indicates the dimensional parameters.

Momentum equation:

$$U^* \cdot \nabla^* U^* = -\frac{1}{\rho}\nabla^* p^* + v\left(\nabla^{*2} U^*\right) + \beta_t g\left(T^* - T_g^*\right) + \beta_c g\left(C^* - C_g^*\right) \tag{2}$$

where β, ρ, and v are the volumetric expansion coefficient, density, and kinematic viscosity of working fluid, respectively.

It should be mentioned that the terms $\beta_t g\left(T^* - T_g^*\right)$ and $\beta_c g\left(C^* - C_g^*\right)$ can be ignored for the momentum equation in x-direction.

Energy balance equation:

$$\left(U^* \cdot \nabla^* T^*\right) = \frac{k}{\rho C_p}\left(\nabla^{*2} T^*\right) \tag{3}$$

In this equation, C_p and k are the heat capacity and the thermal conductivity of the working fluid, respectively.

Concentration balance equation:

$$\left(U^* \cdot \nabla^* C^*\right) = D_{AB}\left(\nabla^{*2} C^*\right) \tag{4}$$

In this equation, D_{AB} indicates the mass diffusivity of the vapor.

Dimensionless form

Governing Eqs. 1–4 can be presented in the dimensionless forms by introducing the following non-dimensional parameters:

$$\nabla = \frac{\nabla^*}{H_{ave}}, \quad U = \frac{U^* H_{ave}}{\alpha}, \quad p = \frac{P^* H_{ave}^2}{\alpha^2 \rho}, \quad T = \frac{T^* - T_g^*}{T_w^* - T_g^*}, \quad C = \frac{C^* - C_g^*}{C_w^* - C_g^*} \tag{5}$$

H_{ave} is the average height of the solar still ($H_{ave} = \frac{H_l + H_r}{2}$). Moreover, α indicates the thermal diffusivity of the working fluid.

The non-dimensional forms of Eqs. 1–4 are:

Continuity equation:

$$\nabla \cdot U = 0 \tag{6}$$

Momentum equation:

$$U \cdot \nabla U = -\nabla p + \mathrm{Pr}\left(\nabla^2 U\right) + Ra\,\mathrm{Pr}(T + BrC) \tag{7}$$

Note that the term $Ra\,\mathrm{Pr}(T + BrC)$ can be ignored for the momentum equation in x-direction.

Energy balance equation:

$$(U \cdot \nabla T) = \left(\nabla^2 T\right) \tag{8}$$

Concentration balance equation:

$$(U \cdot \nabla C) = \frac{1}{Le}\left(\nabla^2 C\right) \tag{9}$$

In these equations, Le, Pr, and Ra are Lewis, Prandtl, and Rayleigh numbers, respectively. Moreover, Br is the buoyancy ratio. These parameters can be defined by:

$$Le = \frac{\alpha}{D_{AB}}, \quad Pr = \frac{v}{\alpha}, \quad Ra = \frac{g\beta_{th}\left(T_w^* - T_g^*\right)H_{ave}^3}{\upsilon\alpha}, \quad Br = \frac{\beta_c\left(C_w^* - C_g^*\right)}{\beta_{th}\left(T_w^* - T_g^*\right)} \tag{10}$$

Boundary conditions

The equations, presented in the prior section, are subjected to the following boundary conditions.

The no-slip velocity, constant temperature, and saturation concentration are used as the boundary conditions on the glass ceiling. These boundary conditions can be presented in the following forms:

$$U^* = 0, \quad T^* = T_g^*, \quad C^* = C^*|_{T^* = T^*_{g,\phi=100\%}} \tag{11}$$

The sidewalls are insulated in terms of heat transfer and concentration. Moreover, no-slip velocity boundary condition is used on them. These boundary conditions are:

$$U^* = 0, \quad \frac{\partial T^*}{\partial x^*} = 0, \quad \frac{\partial C^*}{\partial x^*} = 0 \tag{12}$$

Similar to the glass ceiling, the following boundary conditions are used on the water surface (bottom wall of the computational domain):

$$U^* = 0, \quad T^* = T_w^*, \quad C^* = C^*|_{T^* = T^*_{w,\phi=100\%}} \tag{13}$$

Entropy generations

The following relationships are used to calculate different types of irreversibility in this study.

The local volumetric viscous irreversibility, $S_{g,v}^*$, is defined as follows [35]:

$$S_{g,v}^* = \frac{2\mu}{T^*}\left[\left(\frac{\partial u^*}{\partial x^*}\right)^2 + \left(\frac{\partial v^*}{\partial y^*}\right)^2\right] + \frac{\mu}{T^*}\left[\left(\frac{\partial u^*}{\partial y^*}\right) + \left(\frac{\partial v^*}{\partial x^*}\right)\right]^2 \tag{14}$$

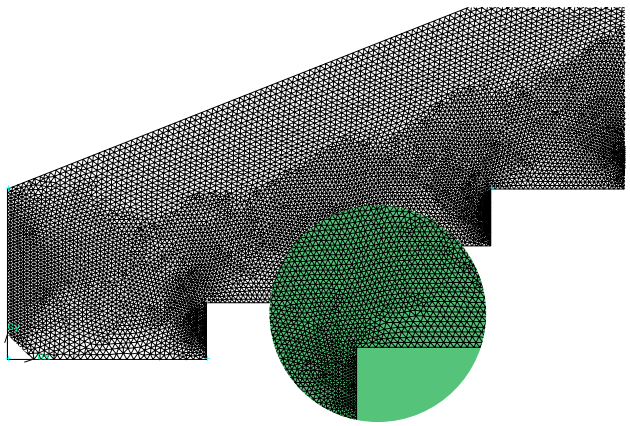

Fig. 2 Typical meshes generated inside the stepped solar still with a near view around one step

In this equation, μ is the viscosity of the working fluid.

The local volumetric thermal irreversibility, $S^*_{g,th}$, is given by [35]:

$$S^*_{g,th} = \frac{k}{T^{*2}}\left[\left(\frac{\partial T^*}{\partial x^*}\right)^2 + \left(\frac{\partial T^*}{\partial y^*}\right)^2\right] \quad (15)$$

The local volumetric concentration irreversibility, $S^*_{g,c}$, can be written in the following form [36]:

$$S^*_{g,c} = \frac{RD}{C^*}\left[\left(\frac{\partial C^*}{\partial x^*}\right)^2 + \left(\frac{\partial C^*}{\partial y^*}\right)^2\right] + \left(\frac{RD}{T}\right)\left[\left(\frac{\partial T^*}{\partial x^*}\right)\left(\frac{\partial C^*}{\partial x^*}\right) + \left(\frac{\partial T^*}{\partial y^*}\right)\left(\frac{\partial C^*}{\partial y^*}\right)\right] \quad (16)$$

where D and R are the mass diffusivity and gas constant, respectively.

The average irreversibility, $\bar{S}_g$, can be obtained by using the following surface integral:

$$\bar{S}_g = \frac{1}{A}\left[\int S_g dA\right] \quad (17)$$

where A indicates the surface of the solar still.

Finally, the Bejan number, Be, can be defined by [35]:

$$Be = \frac{S^*_{g,th}}{S^*_{g,v} + S^*_{g,th} + S^*_{g,c}} \quad (18)$$

Numerical procedure

In this study, a finite volume technique is employed for solving the continuity, momentum, energy, and concentration equations with their boundary conditions. The upwind and central difference schemes with second-order accuracies are selected to discretize the convection and diffusion terms in the governing equations, respectively. The coupling between the velocity and pressure is achieved by employing the SIMPLE algorithm [37]. After discretization of the equations, a line-by-line Thomas algorithm is used to solve the governing equations iteratively. All iterations are continued until the residuals of continuity, momentum, and concentration equations are decreased less than 10^{-3}. However, the convergence criterion for the energy equation is 10^{-6}. The simulations are carried out by the commercial software Ansys Fluent.

Details of mesh and independent solutions

The mesh distribution inside the solar still is shown in Fig. 2. It is observed that an unstructured mesh is used in this study. A close view of meshes generated around a step of the solar still is also illustrated in Fig. 2. Generally, the meshes are very dense near the walls and steps of the solar still, where the velocity, temperature, and concentration gradients are high.

To provide the balancing between the prediction accuracy and running time, the mesh independence of the numerical solutions should be checked attentively. In this study, three mesh numbers, including 15,000, 30,000, and 60,000, are investigated to ensure that the solutions are independent from the mesh number. These mesh numbers are generated inside the solar still with four steps. For each mesh number, different types of irreversibilities are calculated and the results are provided in Table 2 for h = 2 cm, T_g = 39 °C, and T_w = 44 °C. It is clearly found that the percentage differences between the irreversibilities calculated by the mesh numbers of 30,000 and 60,000 are not significant. These percentage differences are up to 0.3%, 0.4%, and 0.3% for the viscous, thermal, and concentration irreversibilities, respectively. Accordingly, to minimize the time of solution and to balance the computational cost and the accuracy of the solution, the mesh number of 30,000 is selected for the rest of computations.

Validation of numerical solution

Prior to performing the required computations, it is important to validate the numerical method. In this investigation, the results of current numerical method are compared with the data reported by Rahbar and Esfahani [38] for a single-slope solar still. The operating conditions and geometrical details of five cases considered for the validation are provided in Table 3. Figure 3 illustrates the results of validation for the mean Nusselt number at different cases listed in Table 3. It can be found that two results are very close and this confirms that the current numerical method has good accuracy.

The mean Nusselt number is obtained by [38]:

Table 2 Grid independence study for the solar still with four steps at h = 2 cm, T_g = 39 °C, and T_w = 44 °C

Mesh number	$S^*_{g,v} \times 10^5$	Percentage difference/%	$S^*_{g,th} \times 10^2$	Percentage difference/%	$S^*_{g,c} \times 10^8$	Percentage difference/%
150,000	2.040	1.2	3.384	1.1	2.367	1.4
300,000	2.065	0.3	3.421	0.4	2.400	0.3
600,000	2.071	–	3.435	–	2.407	–

Table 3 Operating conditions and geometrical details of the cases considered for the validation

Cases	T_w/ °C)	T_g/ °C	Length/ cm	Left side/cm	Right side/cm
1	40	30	98	10	47
2	50	40	98	10	47
3	60	50	98	10	47
4	70	60	98	10	47
5	63	48	43.8	7.5	18.7

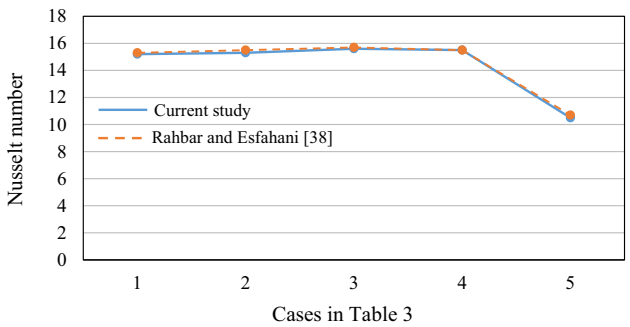

Fig. 3 Comparison between the current numerical results and the data reported by Rahbar and Esfahani [38] for a single-slope solar still

$$\overline{Nu} = \left(\frac{-H}{L\left(T^*_w - T^*_g\right)}\right) \int_0^L \left.\frac{\partial T^*}{\partial n^*}\right|_{wall} dx^* \quad (19)$$

Note that in this equation, n is the perpendicular direction to the wall.

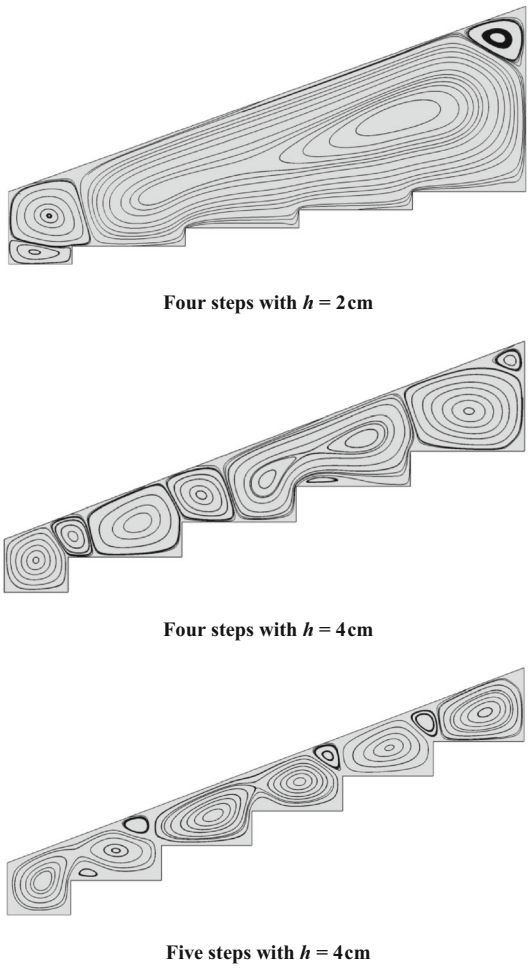

Fig. 4 Effects of number and height of steps on the streamlines in the solar still at T_g = 39 °C and T_w = 44 °C

Results and discussion

In this section, the results of numerical simulations are reported and discussed. All results are presented for two numbers of step, four step heights, and three temperatures of glass ceiling and water surfaces. The effects of these parameters on the streamlines, temperature and concentration fields, viscous, thermal, concentration irreversibilities, and Bejan number are investigated.

The effects of number and height of steps on the streamlines in the solar still at T_g = 39 °C and T_w = 44 °C are shown in Fig. 4. It can be seen that for the case of solar still with four steps and h = 2 cm, four vortices are generated inside the solar still due to both mass and thermal buoyancy forces. These vortices transfer the heat and mass between the water surface and glass ceiling, and

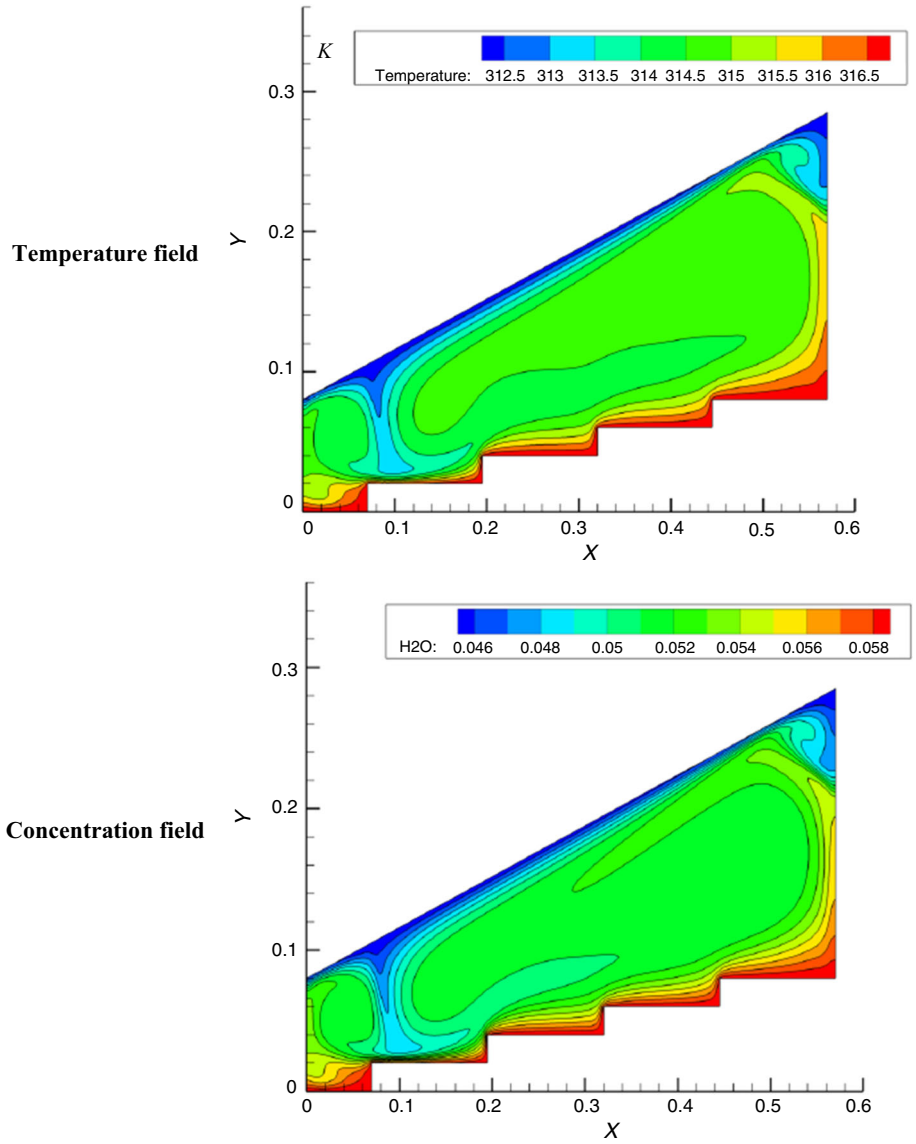

Fig. 5 Temperature and concentration fields in a stepped solar still with four steps at h = 2 cm, T_g = 39 °C, and T_w = 44 °C

accordingly, the operation of the solar still is directly related to them. One of these vortices has larger size, and most space of the solar still is occupied by this vortex. Generally, formation of larger vortex is an inappropriate factor in the solar still as it can increase the heat and mass exchange duration between the evaporation and condensation surfaces [39, 40]. This has negative influence on the productivity of solar still. As a result, the formation of vortices with smaller sizes is favorable. The big vortex breaks down into some smaller vortices with increasing the height of steps. For the case of solar still with four steps and h = 4 cm, there are seven vortices inside the solar still, which have smaller size. The regularity of circulation cells inside the solar still declines with increasing the number of steps. For the solar still with five steps, the vortices have limited space for the rotation.

Figure 5 illustrates the temperature and concentration fields in a solar still with four steps at h = 2 cm, T_g = 39 °C, and T_w = 44 °C. As shown in this figure, the temperature of moist air and concentration of water have no significant changes at the central region of the solar still, while there are steep changes in the temperature and concentration in thin boundary layers close the bottom and top surfaces. Note that the phase changes occur, and most of heat and mass are transferred near these surfaces in the solar still. Thus, these regions have high gradients. The temperature and concentration lines are perpendicular to the sidewalls of the solar still due to the adiabatic assumption on these walls.

Figure 6 shows the contours of viscous, thermal, and concentration irreversibilities in a solar still with four and five steps at h = 3 cm, T_g = 39 °C, and T_w = 44 °C. It can be noticed that the maximum values of all types of

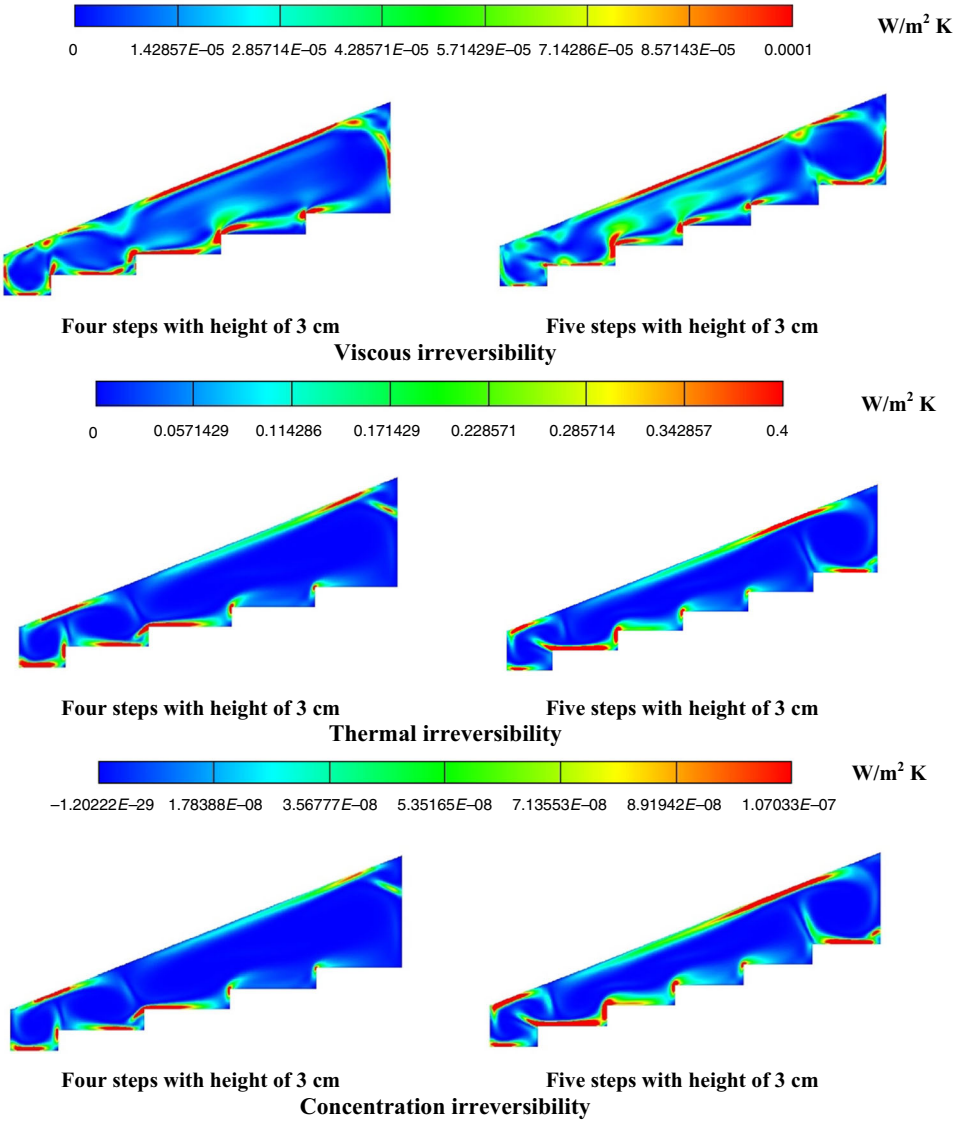

Fig. 6 Contours of viscous, thermal, and concentration irreversibilities in a solar still with four and five steps at h = 3 cm, T_g = 39 °C, and T_w = 44 °C

irreversibilities are generated near the glass ceiling and the water surface of the solar still. These results can be justified by Fig. 5, where one can see that the high temperature and concentration gradients occurred around the glass ceiling and water surface. These large gradients are playing aiding roles on generation of the viscous and concentration irreversibilities. Generally, in the double diffusive free convection, the velocity gradients are larger near the areas where the concentration and thermal gradients are high. Note that in the areas with high concentration and thermal gradients, the fluid can accelerate due to the activation of the mass and thermal buoyancy forces as a necessity of mass conservation [41]. As a consequence, the velocity gradient is also high near the glass ceiling and water surface. Expectedly, the thermal and concentration irreversibilities are near zero around the adiabatic sidewalls of the solar still. However, the viscous irreversibility is high near the sidewalls. The position and maximum value of irreversibilities have remained nearly unchanged inside the solar still by changing the number of steps. Finally, by comparing the order of different types of irreversibility, it can be concluded that the orders of viscous and concentration irreversibilities are negligible in comparison with the thermal irreversibility.

The Bejan number contour in a solar still with four steps at h = 2 cm, T_g = 39 °C, and T_w = 44 °C is disclosed in Fig. 7. The Bejan number is the ratio of thermal irreversibility to total irreversibility including the summation

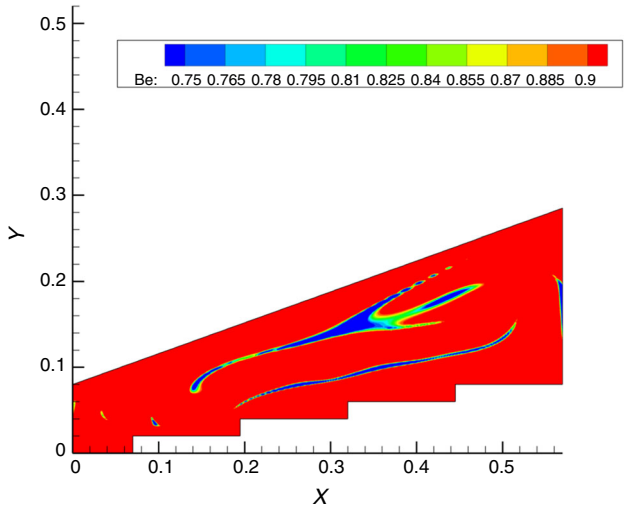

Fig. 7 Bejan number contour in the solar still with four steps at h = 2 cm, T_g = 39 °C, and T_w = 44 °C

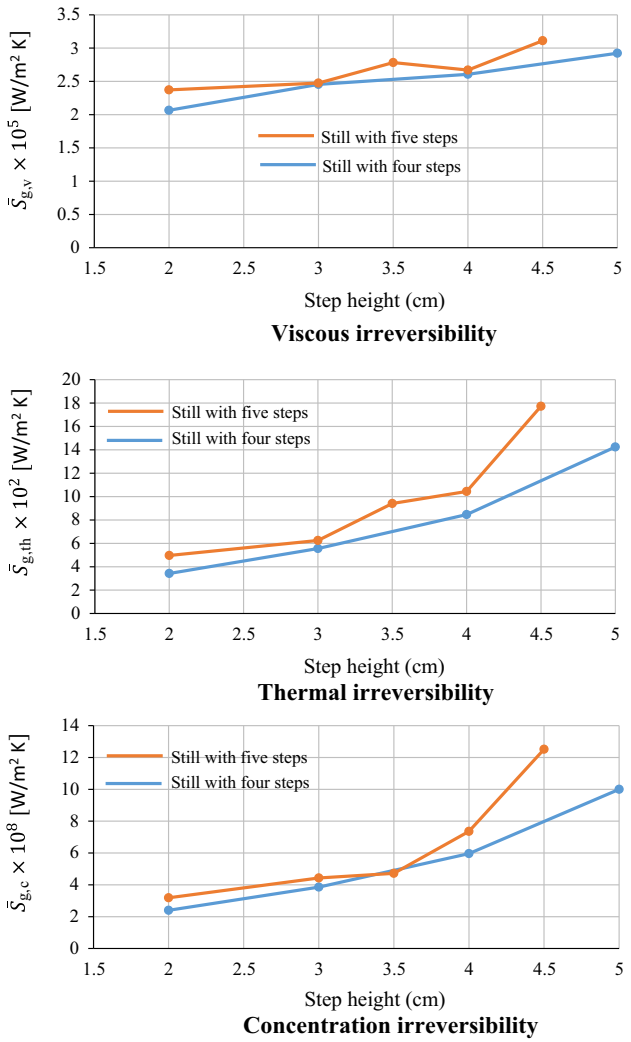

Fig. 8 Viscous, thermal, and concentration irreversibilities for different values of step height and two step numbers at T_g = 39 °C and T_w = 44 °C

of viscous, thermal, and concentration irreversibilities. This number can determine the dominant irreversibility inside the system. From the results, it is evident that the thermal irreversibility is the dominant term in most areas except a narrow region at the center of the solar still. This result is expectable for the laminar regime considered in this study. Generally, the irreversibility due to the heat transfer has significant distribution in a laminar flow in the absence of turbulent fluctuations. However, for a turbulent regime, the fluctuations in the flow can intensify the concentration and velocity gradients and increase the contributions of these irreversibilities.

Figure 8 shows the viscous, thermal, and concentration irreversibilities for different values of step height and two step numbers at T_g = 39 °C and T_w = 44 °C. It can be found that all types of irreversibility increase as the step height increases. For instance, in a solar still with four steps, the viscous, thermal, and concentration irreversibilities increase about 41.55%, 316.43%, and 316.6%, respectively, as the step height increases in the range of 2 cm–5 cm. The distance between the glass ceiling and water surface and generally the space inside the solar still decrease as the height of steps increases. Shorter distance between upper and lower walls provides higher rate of heat and mass transfer between these walls, and accordingly, the fluid flows at higher velocity when the solar still has steps with larger height. In addition, as noticed in Fig. 4, the number of circulation cells increases with increasing the step height. As the number of circulation cells increases, some short-circuit moist air currents are created between two walls and this shortens the duration time for transferring the vapor between the water surface and glass ceiling [40]. Finally, the small distance between the active walls, non-insulated walls, causes more heat and mass penetrations toward the opposite wall. As a result, the transport phenomena are intensified inside a more limited space and this leads to generate more irreversibilities inside a stepped solar still with larger step height. Figure 9 also shows that more irreversibilities are generated inside a solar still with five steps as compared with the still with four steps. For instance, the viscous, thermal, and concentration irreversibilities increase about 14.77%, 45.03%, and 32.82%, respectively, by using five steps with height of 2 cm instead of four steps with the same height in the stepped solar still. As mentioned earlier, some irregular vortices are generated inside the solar still with five steps. These irregular vortices distort the concentration and temperature distributions and disrupt the flow driven in the solar still, which render the increase in the irreversibilities.

The effects of temperatures of the glass ceiling and water surface on the viscous, thermal, and concentration irreversibilities inside a solar still with five steps at h = 3.5 cm are illustrated in Fig. 9. This figure exhibits

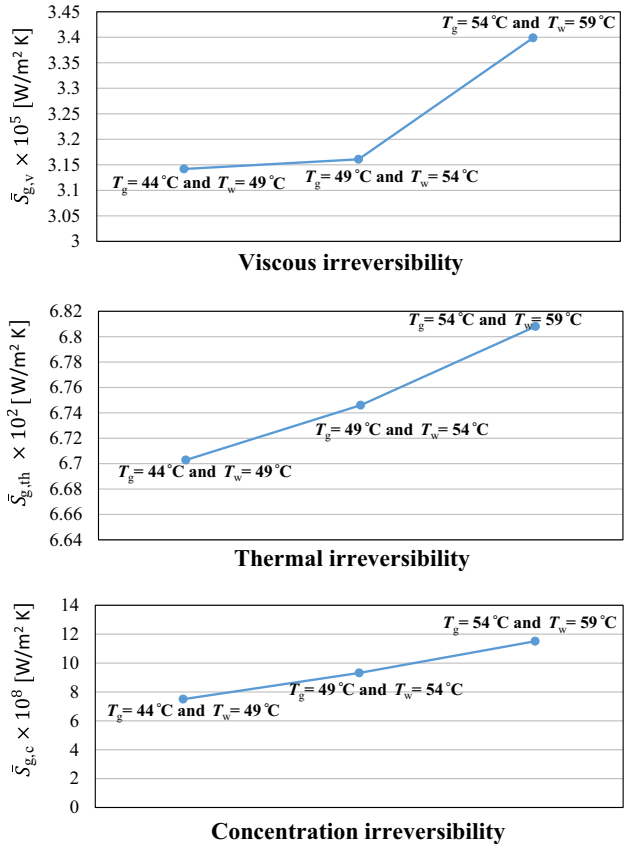

Fig. 9 Effects of operating temperatures on the viscous, thermal, and concentration irreversibilities inside a solar still with five steps at h = 3.5 cm

that all types of irreversibility increase by increasing the temperatures on the glass ceiling and water surface. The viscous, concentration, and thermal irreversibilities increase about 8.2%, 53.5%, and 1.57%, respectively, by increasing the temperatures of the glass ceiling and water surface from T_g = 44 °C and T_w = 49 °C to T_g = 54 °C and T_w = 59 °C. As presented in Table 1, the thermophysical properties of the moist air, working fluid are related to the temperatures of the glass ceiling and water surface. Increasing these temperatures boosts the viscosity of the moist air and leads to generate more frictional force and subsequently larger viscous irreversibility inside the solar still. The thermal conductivity of moist air increases with increasing the operating temperature of the solar still. In addition, the moist air becomes less dense and can easily rise as its temperature increases. Accordingly, more heat and mass can be exchanged between the water surface and glass ceiling. These enhancements in heat and mass transfer intensify the concentration and temperature gradients in the flow field and lead to increase in the concentration and thermal irreversibilities.

Conclusions

The aim of this numerical study was to improve the design of a stepped solar still based on the entropy generation minimization. The effects of step number, step height, and temperatures on the glass ceiling and water surfaces on the flow structure, temperature and concentration fields, and different irreversibilities were investigated. From this study, the following conclusions are achieved:

- It is clearly realized that the number and height of the steps have considerable effects on the buoyancy-driven vortices.
- The temperature of moist air and concentration of water have no significant changes at the central region of the solar still, while there are steep changes in the temperature and concentration in thin boundary layers close the bottom and top surfaces.
- The active sites for generating irreversibilities are regions near the evaporation and condensation surfaces inside the solar still.
- All types of irreversibility are intensified by increasing the number or height of the steps.
- In a solar still with four steps, the viscous, thermal, and concentration irreversibilities increase about 41.55%, 316.43%, and 316.6%, respectively, as the step height increases in the range of 2–5 cm.
- From the view point of irreversibility minimization, the usage of a stepped solar still with lower operating temperatures is recommended.
- The viscous, concentration, and thermal irreversibilities increase about 8.2%, 53.5%, and 1.57%, respectively, by increasing the temperatures of the glass ceiling and water surface from T_g = 44 °C and T_w = 49 °C to T_g = 54 °C and T_w = 59 °C.
- The thermal irreversibility is the dominant term in most areas except a narrow region at the center of the solar still.

For the future research in this field, it is recommended to focus on the usage of some techniques for improving the productivity of the stepped solar still. For instance, the thermoelectric modules can be used to improve the evaporation and condensation rates inside the stepped solar stills.

References

1. Nayi KH, Modi KV. Pyramid solar still: a comprehensive review. Renew Sustain Energy Rev. 2018;81:136–48.
2. Selvaraj K, Natarajan A. Factors influencing the performance and productivity of solar stills—a review. Desalination. 2018;435:181–7.

3. Rashidi S, Karimi N, Mahian O, Esfahani JA. A concise review on the role of nanoparticles upon the productivity of solar desalination systems'. J Therm Anal Calorim. 2019;132:1145–59.
4. Xuan L, Arunkumar T, Raj K, Rufuss DDW, Denkenberger D, Tingting G, Velraj R. A review of efficient high productivity solar stills. Renew Sustain Energy Rev. 2019;101:197–220.
5. Bait O, Si-Ameur M. Enhanced heat and mass transfer in solar stills using nanofluids: a review. Sol Energy. 2018;170:694–722.
6. Omara ZM, Abdullah AS, Kabeel AE, Essa FA. The cooling techniques of the solar stills' glass covers—a review. Sol Energy. 2017;78:176–93.
7. Shukla A, Kant K, Sharma A. Solar still with latent heat energy storage: a review. Innov Food Sci Emerg Technol. 2017;41:34–46.
8. Rashidi S, Rahbar N, Valipour MS, Esfahani JA. Enhancement of solar still by reticular porous media: experimental investigation with exergy and economic analysis'. Appl Therm Eng. 2018;130:1341–8.
9. Manokar AM, Winston DP. Experimental analysis of single basin single slope finned acrylic solar still'. Mater Today: Proc. 2017;4:7234–9.
10. Kabeel AE, Omara ZM, Younes MM. Techniques used to improve the performance of the stepped solar still—a review. Renew Sustain Energy Rev. 2015;46:178–88.
11. Abdallah S, Badran O, Mazen Abu-Khader M. Performance evaluation of a modified design of a single slope solar still'. Desalination. 2008;219:222–30.
12. Omara ZM, Kabeel AE, Younes MM. Enhancing the stepped solar still performance using internal reflectors. Desalination. 2013;314:67–72.
13. Abdullah AS. Improving the performance of stepped solar still'. Desalination. 2013;319:60–5.
14. Rashidi S, Bovand M, Rahbar N, Esfahani JA. Steps optimization and productivity enhancement in a nanofluid cascade solar still'. Renew Energy. 2018;118:536–45.
15. Saadi Z, Rahmani A, Lachtar S, Soualmi H. Performance evaluation of a new stepped solar still under the desert climatic conditions. Energy Convers Manag. 2018;171:1749–60.
16. Naroei M, Sarhaddi F, Sobhnamayan F. Efficiency of a photovoltaic thermal stepped solar still: experimental and numerical analysis. Desalination. 2018;441:87–95.
17. Torabi M, Zhang K, Karimi N, Peterson GP. Entropy generation in thermal systems with solid structures—a concise review. Int J Heat Mass Transf. 2016;97:917–31.
18. Sciacovelli A, Verda V, Sciubba E. Entropy generation analysis as a design tool—a review. Renew Sustain Energy Rev. 2015;43:1167–81.
19. Bahiraei M, Jamshidmofid M, Amani M, Barzegarian R. Investigating exergy destruction and entropy generation for flow of a new nanofluid containing graphene–silver nanocomposite in a micro heat exchanger considering viscous dissipation. Powder Technol. 2018;336:298–310.
20. Bahiraei M, Heshmatian S. 'Efficacy of a novel liquid block working with a nanofluid containing graphene nanoplatelets decorated with silver nanoparticles compared with conventional CPU coolers'. Appl Therm Eng. 2017;127:1233–45.
21. Bahiraei M, Heshmatian S. Application of a novel biological nanofluid in a liquid block heat sink for cooling of an electronic processor: thermal performance and irreversibility considerations. Energy Convers Manag. 2017;149:155–67.
22. Ebrahimi-Moghadam A, Jabari Moghadam A. Optimal design of geometrical parameters and flow characteristics for Al2O3/water nanofluid inside corrugated heat exchangers by using entropy generation minimization and genetic algorithm methods. Appl Therm Eng. 2019;149:889–98.
23. Ghanbarpour M, Khodabandeh R. Entropy generation analysis of cylindrical heat pipe using nanofluid'. Thermochim Acta. 2015;610:37–46.
24. Sivaraj C, Sheremet MA. MHD natural convection and entropy generation of ferrofluids in a cavity with a non-uniformly heated horizontal plate. Int J Mech Sci. 2018;149:326–37.
25. Bouchoucha A, Bessaïh R, Oztop HF, Al-Salem K, Bayrak F. Natural convection and entropy generation in a nanofluid filled cavity with thick bottom wall: effects of non-isothermal heating. Int J Mech Sci. 2017;126:95–105.
26. Bahiraei M, Mazaheri N, Aliee F. Second law analysis of a hybrid nanofluid in tubes equipped with double twisted tape inserts. Powder Technol. 2019;345:692–703.
27. Bahiraei M, Mazaheri N. Second law analysis for flow of a nanofluid containing graphene–platinum nanoparticles in a minichannel enhanced with chaotic twisted perturbations. Chem Eng Res Des. 2018;136:230–41.
28. Rahman MM, Öztop HF, Ahsan A, Kalam MA, Varol Y. Double-diffusive natural convection in a triangular solar collector. Int Commun Heat Mass Transfer. 2012;39:264–9.
29. Javaniyan Jouybari H, Saedodin S, Zamzamian A, Eshagh Nimvari M. Experimental investigation of thermal performance and entropy generation of a flat-plate solar collector filled with porous media. Appl Therm Eng. 2017;127:1506–17.
30. Rashidi S, Javadi P, Esfahani JA. Second law of thermodynamics analysis for nanofluid turbulent flow inside a solar heater with the ribbed absorber plate. J Therm Anal Calorim. 2019;135:551–63.
31. Rashidi S, Akar S, Bovand M, Ellahi R. Volume of fluid model to simulate the nanofluid flow and entropy generation in a single slope solar still. Renew Energy. 2018;115:400–10.
32. Rashidi S, Esfahani JA. Spatial entropy generation analysis for the design improvement of a single slope solar still. Environ Prog Sustain Energy. 2018;37:1112–20.
33. Clark JA. The steady state performance of a solar still. Sol Energy. 1990;44:43–9.
34. Rahbar N, Esfahani JA. Productivity estimation of a single-slope solar still: theoretical and numerical analysis. Energy. 2013;49:289–97.
35. Bejan A. Entropy generation through heat and fluid flow. New York: Wiley; 1982.
36. Magherbi M, Abbassi H, Hidouri N, Ben Brahim A. Second law analysis in convective heat and mass transfer. Entropy. 2006;8:1–17.
37. Patankar SV. Numerical heat transfer and fluid flow. New York: Hemisphere; 1980.
38. Rahbar N, Esfahani JA. Estimation of convective heat transfer coefficient in a single-slope solar still: a numerical study. Desalin Water Treat. 2012;50:387–96.
39. Edalatpour M, Kianifar A, Ghiami S. Effect of blade installation on heat transfer and fluid flow within a single slope solar still. Int Commun Heat Mass Transf. 2015;66:63–70.
40. Rashidi S, Bovand M, Esfahani JA. Optimization of partitioning inside a single slope solar still for performance improvement. Desalination. 2016;395:79–91.
41. Oliveski RDC, Macagnan MH, Copetti JB. Entropy generation and natural convection in rectangular cavities. Appl Therm Eng. 2009;29:1417–25.